Nuclear Engineering and Technology 52 (2020) 1597–1601

Contents lists available at ScienceDirect

Nuclear Engineering and Technology

journal homepage: www.elsevier.com/locate/net

Technical Note

Determination of defect depth in industrial radiography imaging using MCNP code and SuperMC software

Abdollah Khorshidi [a, b, *], Behzad Khosrowpour [c], S. Hamed Hosseini [c]

[a] School of Paramedical, Gerash University of Medical Sciences, Gerash, Iran
[b] Medical Radiation Engineering Department, Parand Branch, Islamic Azad University, Parand, Iran
[c] Medical Radiation Engineering Department, Science and Research Branch, Islamic Azad University, Tehran, Iran

ARTICLE INFO

Article history:
Received 1 September 2019
Received in revised form
8 December 2019
Accepted 10 December 2019
Available online 11 December 2019

Keywords:
Industrial radiography
Defect depth
Weld
Gamma flux
MCNP
SuperMC

ABSTRACT

Background: Non-destructive evaluation of defects in metals or composites specimens is a regular method in radiographic imaging. The maintenance examination of metallic structures is a relatively difficult effort that requires robust techniques for use in industrial environments.
Methods: In this research, iron plate, lead marker and tungsten defect with a 0.1 cm radius in spherical shape were separately simulated by MCNP code and SuperMC software. By ^{192}Ir radiation source, two exposures were considered to determine the depth of the actual defined defect in the software. Also by the code, displacement shift of the defect were computed derived from changing the source location along the x- or y-axis.
Results: The computed defect depth was identified 0.71 cm in comparison to the actual one with accuracy of 13%. Meanwhile, the defect position was recognized by disorder and reduction in obtained gamma flux. The flux amount along the x-axis was approximately 0.5E+11 units greater than the y-axis.
Conclusion: This study provides a method for detecting the depth and position of the defect in a particular sample by combining code and software simulators.

1. Introduction

The materials must be tested before construction and use on structures. Therefore, the design should be such that effective inspection and data acquisition is possible during the maintenance and servicing of a piece or equipment at different stages of construction. In addition to the visual inspection method, the five basic methods of non-destructive testing are: magnetic particles, penetrating fluids, radiography (X or gamma-rays), ultrasonic, and eddy currents. Non-destructive testing is the testing of a substance without destruction or elimination. The radiographic and ultrasound tests can easily detect flaws besides internal structure inside the matter. The accuracy of interpreting non-destructive methods requires special skills and knowledge that the interpreter can derive from formulated techniques and guidelines. Industrial radiography has been steadily evolving for more than a century [1–4]. In industrial radiography, the usual method of generating a radiograph is to apply a penetrating radiation source such as X- or gamma-ray on one side of the piece and place the detector or radiographic film on the other side. The energy of the beam should be large enough to pass through the piece and reach the film. The radiation source is physically small (a few millimeters in diameter) and the incident rays traverse the sample toward the detector, producing a clear image of the defects, edges of the piece and sample discontinuities [5–11]. In this method a variety of internal defects such as cracks, gas cavities, imprinted slag, penetration of external materials like tungsten and welding slag, and non-melting and mixing are visible and detected [12–14]. In this research, an industrial radiographic imaging technique is simulated using Monte Carlo N-Particle version X (MCNPX) code and SuperMC 3.3 software over hypothetical defect's depth by a piece of tungsten metal besides a lead marker. Both computational simulators are compared to identify the depth and position of the defined defect within a specimen.

2. Materials and methods

The MCNP code is capable of solving particle transport problems

* Corresponding author. School of Paramedical, Gerash University of Medical Sciences, Gerash, Iran.
E-mail address: abkhorshidi@yahoo.com (A. Khorshidi).

https://doi.org/10.1016/j.net.2019.12.010

(photon, neutron, photon and electron transport) [15]. Also, the SuperMC version 3.3 software packages [16] can calculate the radiation issues and its main feature is easy working with no need to know the programming language and backgrounds. In addition to that, this software is licensed and can be cited by important authorities such as the IAEA and all safety centers responsible for collecting and writing nuclear safety standards such as radiation protection (ICRP, ICRU). The software SuperMC has been written by the FDS team based on the Monte Carlo algorithm from the University of Science and Technology of China (USTC).

According to Fig. 1, on the Iron plate (Fe) was placed a lead (Pb) piece as a marker towards the radioactive source. Then on the other side, the radiographic film or detector was located to calculate the gamma-ray flux using the mentioned simulators. The spherical tungsten (W) with a 0.1 cm radius was considered at the center. After that, the simulated scheme is irradiated twice based on Fig. 2 to calculate the defect depth (D) using Eq. (1).

$$D = \frac{t \times S_D}{S_M} \quad \text{(Eq 1)}$$

where t is sample thickness, and S_D and S_M are defect and marker displacements, respectively [17]. Eq. (2) was used to calculate the distance of the Iridium-192 source (E = 316.51 keV of gamma-ray with 82.81% intensity) to the piece with the above specifications [18].

$$F = \frac{t \times (U_T + S)}{U_T} \quad \text{(Eq 2)}$$

where t is sample thickness (cm), U_T is total un-detectability (cm), and S is effective diameter of the source (cm). Meanwhile Table 1 demonstrates the simulated metal plate specimen specifications from Fig. 1. It might be possible to use ^{137}Cs as the source for exposure, but this isotope is always diluted with inactive Cs isotopes. This makes it difficult to obtain a physically small source, and a large volume of the source makes it impossible to detect fine details in a radiographic assessment. The gamma source of ^{192}Ir was simulated in spherical shape at distinct distance from the sample metal as shown in Fig. 2.

Then according to Fig. 3, the problem was simulated again by MCNP code utilizing a radiography tally of F5 (photon numbers per cm^2) to compute the flux at a point. The purpose of this work was to estimate the displacement shift of the defect into the sample and the marker by changing the source location along the x- or y-axis. Subsequently using Eq. (1), the depth of the defect was calculated and compared with the actual defect position so that the relative error and then the accuracy of this method can be estimated.

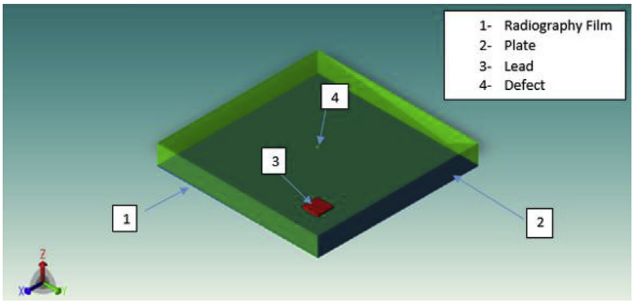

Fig. 1. Problem simulation using SuperMC software including Fe plate, W defect and Pb marker.

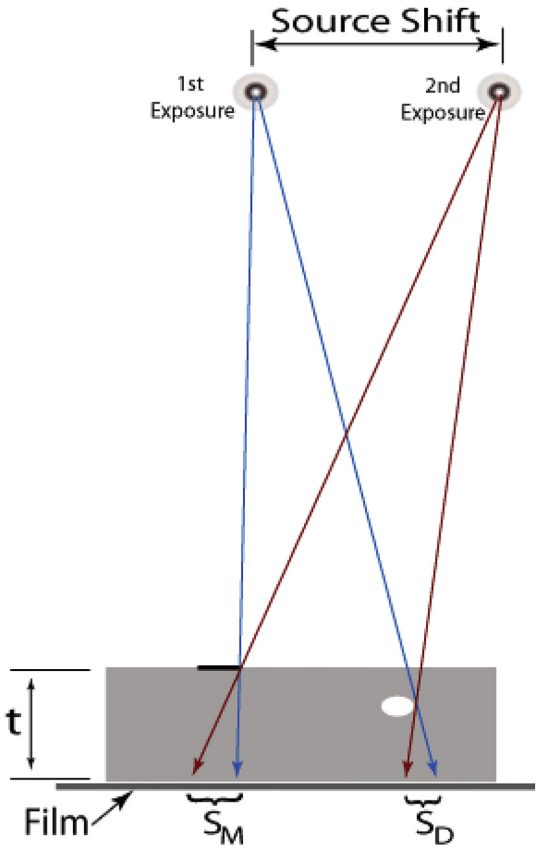

Fig. 2. An overview of calculating defect depth using industrial radiography in twice exposure.

3. Results

The graph of gamma flux emitted from the ^{192}Ir source within the piece using SuperMC software has been shown in Fig. 4. The distribution of gamma flux in iron plate is nearly integrated and seamless, which makes it easy to detect the lead marker in the corner. Meanwhile, the radiographic output obtained from the MCNP code for two exposures has been shown in Fig. 5 to calculate the displacement of the defect and the marker by the source movement. It can be seen that the radiography tally distinguishes the tungsten impurities and the lead marker from the iron sample piece. Because the marker is a lead, so a large number of gamma rays are absorbed by the lead before reaching the iron sample. As a result, it is easy to calculate the displacements whose values have been given in Table 2.

Using the F5 tally in the MCNP code, the gamma flux emitted from ^{192}Ir was computed within and around the defined defect inside the specimen. As can be seen from Fig. 6, it can be concluded that at point x = −0.5, y = −0.5 there is a disturbance in the flux process, which is the defect position within the specimen. The obtained gamma flux decreased from about 9.5E+11 to 6.5E+11 photon/cm^2 along both the x and y axes. After the identified defect position, the flux amount along the x-axis was approximately 0.5E+11 units larger than the y-axis. The aim of the procedure was to confirm Eq. (1) method as well as the radiography-tally method.

4. Discussion

Industrial radiography for non-destructive testing is normally applied for inspecting concrete [19] and a plurality of welds, for

Table 1
Technical specifications of the problem in simulation.

Label	Material	Physical Dimensions (cm)
Source	Ir-192	0.2
Sample metal	Iron (Fe)	10 × 10 × 1.21
Sample marker	Lead (Pb)	1 × 1 × 0.1
Defect	Tungsten (W)	0.1
The actual defect (tungsten) position within the sample piece	X = −0.5, Y = −0.5, Z = 0.5	

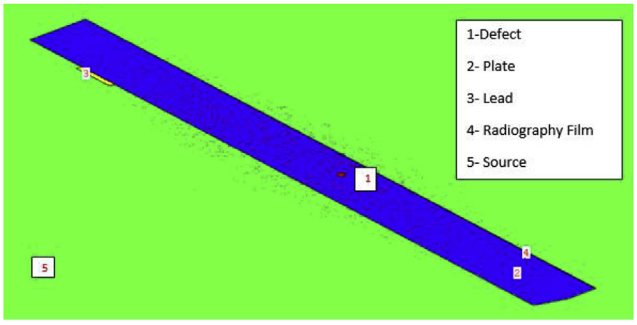

Fig. 3. Problem simulation using MCNP code including Fe plate, W defect and Pb marker.

example in components and storage tanks, water and gas pipes [20]. This method can recognize flaws or cracks that might otherwise not be visible. These properties have made the non-destructive technique as a main instrument for reliability, safety and quality control. In some applications, the characterizing of high energy penetrating radiation has some limitations resulting from the geometry and materials of the detector in the obtained final signal. Therefore, utilizing other radiation like neutron [21] or electron [22] beams as a combined method may compensate or complete the shortcomings of X or gamma-ray method. Also, induced beam production from other reactions can be suggested where large radiographic counters cannot be implemented.

The energy of gamma rays from the source must be sufficient to penetrate the thickness of the specimen to be radiographed. In the literature, useful thickness ranges of metals are available for different gamma ray sources. As the energy of emitted radiation is the property of the source and cannot be altered, the only way to generate different energy radiation is to use another source. Thus, ^{60}Co is a hard metal with density of 8.9 g/cm^3, a half life of 5.3 years and two gamma photons in cascade with energy of 1.17 and 1.33 MeV. Besides, ^{192}Ir is very hard metal of platinum family with density of 22.4 g/cm^3, a half life of 74.4 days, and a complex spectrum of gamma rays containing at least 24 spectral lines of 0.13, 0.29, 0.58, 0.60 and 0.61 MeV. The thickness range for which the source can be utilized is about 100 mm steel. On the other hand, ^{137}Cs is one of the most common fission products of the atomic pile; the radioactive salt is compressed to a density of 3.5 g/cm^3 by a 0.662 MeV gamma ray. Cs is chiefly used for the radiography of steel thickness between 40 and 100 mm [17].

Radiation inspection control systems for cargo and freight containers typically use transmission techniques with a fan beam [23] to produce images of a target object. Nazemi et al. [4] have predicted a pixel value's non-uniformity in tangential and polar angles via artificial neural network at the range of 100–300 kVp of X-ray tube by 23% mean relative error. Meanwhile, Machado et al. [24] have designed a planar eddy current array probe by 4 m/s with 3 mm lift-off in inspection of low conductivity unidirectional carbon fiber reinforced polymer (CFRP) [25] ropes to detect the 0.1 cm defect with an excellent signal to noise ratio (SNR). Moreover, nano-scale materials play a significant role in power industry [26]

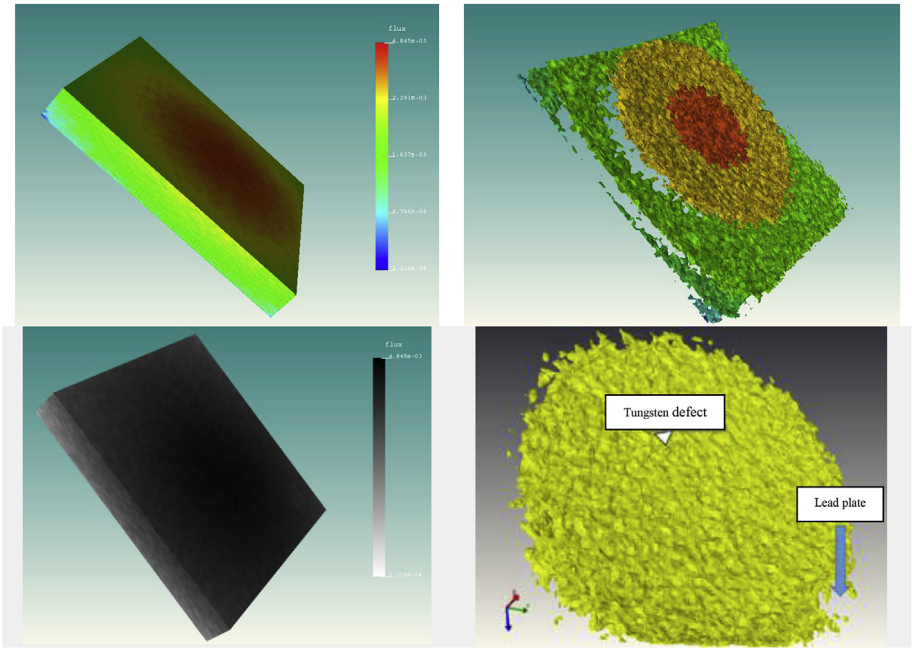

Fig. 4. The obtained gamma flux distribution from SuperMC software.

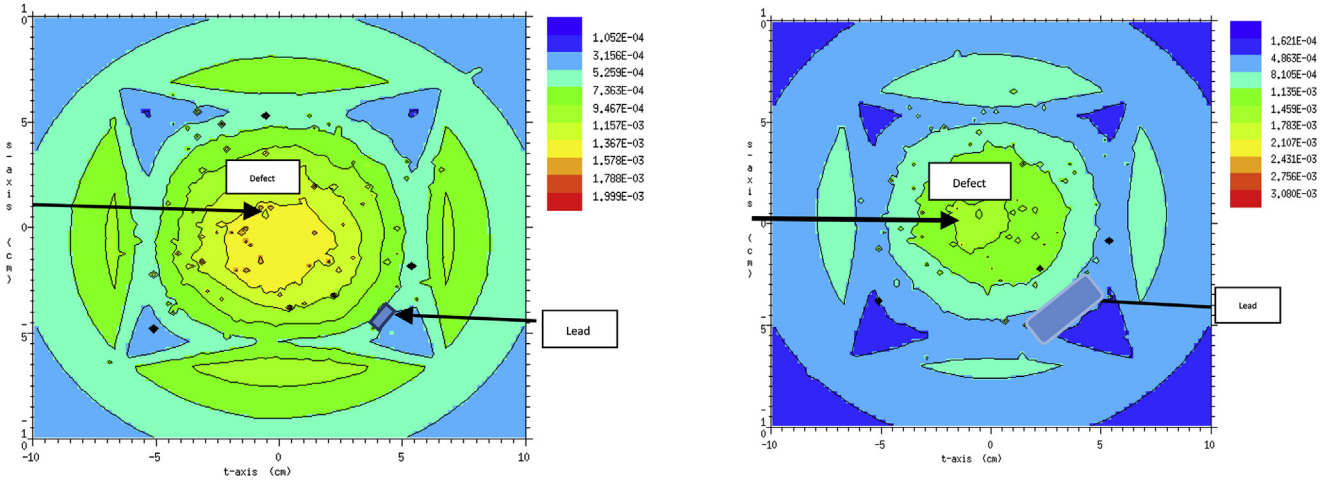

Fig. 5. The radiography tally results from MCNP code.

Table 2
The values obtained from MCNP simulation and SuperMC reality.

Parameter	Value (cm)
S_M displacement (by MCNP simulation)	0.85
S_D displacement (by MCNP simulation)	0.50
Computed defect depth (by MCNP simulation)	0.71
Actual defect depth (by SuperMC software and Eq. (1))	0.61

and medicine [27–29] to increase the efficiency and reduce the cost as well as stable provision of energy required. Furthermore, the non-destructive technique is also used in aviation and drones to investigate the aircraft fuselages for damage due to wear, hail-stones, lightning, and bird strikes. Some tests such as displacement or acceleration at different locations of a specimen need to be appraised via the known input or corresponding output by a transfer function [30] to detect the unforeseen instabilities or tolerances.

In this study, the accuracy of determining the depth defect of tungsten in a distinct piece via computed method was 13% compared to the actual defect depth. Since gamma rays were absorbed by the lead marker, the source shift and then the defect position were simply identified. In addition to that, the reduction and disorder in gamma-flux map revealed the precise position of the defect. The major parameters for the reliability evaluation of non-destructive testing are based on the defect length, which can be determined with a reasonable degree of confidence according to the guidelines for standard practices of ASTM E2862 and MIL-HDBK-1823A [31]. The future study will focus on the classification of different types of welding defects in dissimilar distributions to improve the accuracy.

5. Conclusion

This methodological research has provided a procedure of detecting the depth defect in a distinct specimen by combining code and software simulators. This method has suggested the possibility of determining both the size and the depth of the defects in metals or composite caused by any probabilities. Here, computed defect depth was 0.71 cm in comparison to the actual one with accuracy of 13%.

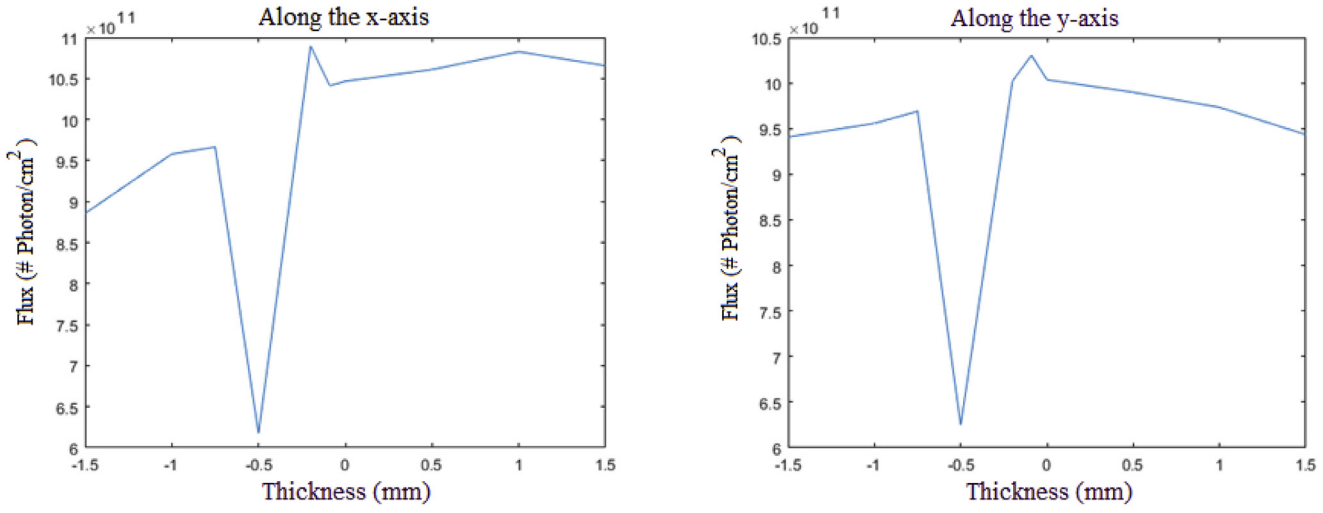

Fig. 6. Changes in gamma flux emitted from ^{192}Ir in terms of sample specimen.

Author disclosures

The authors have declared no conflicts of interest.

Ethical approval

Not required.

Funding source

No Involvement.

Declaration of competing interest

The authors declare that they have no known competing financial interests or personal relationships that could have appeared to influence the work reported in this paper.

References

[1] I. Valavanis, D. Kosmopoulos, Multiclass defect detection and classification in weld radiographic images using geometric and texture features, Expert Syst. Appl. 37 (12) (2010) 7606–7614, https://doi.org/10.1016/j.eswa.2010.04.082.
[2] ASTM E1032-19, Standard Practice for Radiographic Examination of Weldments Using Industrial X-Ray Film, ASTM International, West Conshohocken, PA, 2019, https://doi.org/10.1520/E1032-19. www.astm.org.
[3] Nacereddine N, Zelmat M, Belaïfa SS, Tridi M. Weld defect detection in industrial radiography based digital image processing. 3rd International Conference: Sciences of Electronic, Technologies of Information and Telecommunications March 27-31, 2005 – Tunisia.
[4] E. Nazemi, A. Movafeghi, B. Rokrok, M.H. Choopan Dastjerdi, A novel method for predicting pixel value distribution non-uniformity due to heel effect of X-ray tube in industrial digital radiography using artificial neural network, J. Nondestruct. Eval. 38 (2019) 3, https://doi.org/10.1007/s10921-018-0542-9.
[5] G. De Angelis, M. Meo, D.P. Almond, S.G. Pickering, S.L. Angioni, A new technique to detect defect size and depth in composite structures using digital shearography and unconstrained optimization, NDT E Int. 45 (1) (2012) 91–96, https://doi.org/10.1016/j.ndteint.2011.07.007.
[6] A. Khorshidi, Neutron activator design for 99Mo production yield estimation via lead and water moderators in transmutation's analysis, Instrum. Exp. Tech. 61 (2) (2018) 198–204, https://doi.org/10.1134/S002044121802015X.
[7] J.S. Nabipour, A. Khorshidi, Spectroscopy and optimizing semiconductor detector data under X and γ photons using image processing technique, J. Med. Imaging Radiat. Sci. 49 (2) (2018) 194–200, https://doi.org/10.1016/j.jmir.2018.01.004.
[8] A. Khorshidi, A. Pazirandeh, Molybdenum transmutation via 98Mo samples using bismuth/lead neutron moderators, Europhys. Lett. 123 (1) (2018) 12001, https://doi.org/10.1209/0295-5075/123/12001.
[9] A. Khorshidi, M. Ashoor, S.H. Hosseini, A. Rajaee, Evaluation of collimators' response: round and hexagonal holes in parallel and fan beam, Prog. Biophys. Mol. Biol. 109 (2012) 59–66, https://doi.org/10.1016/j.pbiomolbio.2012.03.003.
[10] A. Khorshidi, J. Soltani-Nabipour, F. Sadeghi, Constructing environmental radon gas detector and measuring concentration in residential buildings, Phys. Part. Nucl. Lett. 16 (6) (2019), https://doi.org/10.1134/S154747711906030X.
[11] A. Khorshidi, Molybdenum-99 production via lead and bismuth moderators and milli-structure-98Mo samples by the indirect production technique using the Monte Carlo method, Phys. Uspekhi 62 (9) (2019) 931–940, https://doi.org/10.3367/UFNe.2018.09.038441.
[12] H. Wirdelius, E. Oesterberg, Study of Defect Characteristics Essential for NDT Testing Methods ET, UT and RT, vol. 42, IAEA, 2000. SKI Report 00.
[13] D. Schumacher, N. Meyendorf, I. Hakim, U. Ewert, Defect recognition in CFRP components using various NDT methods within a smart manufacturing process, in: 44th Annual Review of Progress in Quantitative Nondestructive Evaluation, Volume 37, AIP Conf. Proc., vol. 1949, 2018, https://doi.org/10.1063/1.5031521, 020024-1–020024-11.
[14] M. Kemppainen, I. Virkkunen, Crack characteristics and their importance to NDE, J. Nondestruct. Eval. 30 (3) (2011) 143–157, https://doi.org/10.1007/s10921-011-0102-z.
[15] Los Alamos National Laboratory, MCNPX User's Manual, Version 2.6.0, 2008. April.
[16] FDS-Team, SuperMC User Manual-EN. V 3.3, FDS-Team, 2018.
[17] International Atomic Energy Agency, Industrial Radiography, Manual for the Syllabi Contained in IAEA-TECDOC-628, Training Guidelines in Non-destructive Testing Techniques, IAEA-TCS-3, 1992.
[18] W. Guo, Y. Chen, Research on defect depth measurement algorithm in digital radiography testing, in: 19th World Conference on Non-destructive Testing, 2016.
[19] M. Ashoor, A. Khorshidi, L. Sarkhosh, Introducing a novel coefficient on mixed-nanoparticles material: relationship between the theoretical and experimental densities, Heliyon 5 (7) (2019), e02056, https://doi.org/10.1016/j.heliyon.2019.e02056.
[20] D. Mathijsen, Innovation bottlenecks in non destructive testing, Reinforc Plast 60 (2) (2016) 93–96, https://doi.org/10.1016/j.repl.2016.02.001.
[21] A. Khorshidi, Radiochemical parameters of molybdenum-99 transmutation in cyclotron-based production method using a neutron activator design for nuclear-medicine aims, Eur. Phys. J. Plus 134 (2019) 249, https://doi.org/10.1140/epjp/i2019-12568-3.
[22] A. Khorshidi, A. Rajaee, M. Ahmadinejad, M. Ghoranneviss, M. Ettelaee, Low energy electron generator design and depth dose prediction for micro-superficies tumors treatment purposes, Phys. Scr. 89 (9) (2014), 095001, https://doi.org/10.1088/0031-8949/89/9/095001.
[23] A. Khorshidi, M. Ashoor, S.H. Hosseini, A. Rajaee, Estimation of fan beam and parallel beam parameters in a wire mesh design, J. Nucl. Med. Technol. 40 (1) (2012) 37–43, https://doi.org/10.2967/jnmt.111.089904.
[24] M.A. Machado, K.N. Antin, L.S. Rosado, P. Vilaça, T.G. Telmo Santos, Contactless high-speed eddy current inspection of unidirectional carbon fiber reinforced polymer, Compos. B Eng. 168 (1) (2019) 226–235, https://doi.org/10.1016/j.compositesb.2018.12.021.
[25] M.A. Al-Siddiq Bin Rahman, W.L. Lai, H. Saeedipour, K.L. Goha, Cost-effective and efficient resin-injection device for repairing damaged composites, Reinforc Plast 63 (3) (2019) 156–160, https://doi.org/10.1016/j.repl.2018.11.001.
[26] N.M. Chikhradze, F.D.S. Marquis, G.S. Abashidze, Hybrid fiber and nanopowder reinforced composites for wind turbine blades, J. Mater. Sci. Technol. 4 (1) (2015) 60–67, https://doi.org/10.1016/j.jmrt.2015.01.002.
[27] A. Khorshidi, Gold nanoparticles production using reactor and cyclotron based methods in assessment of 196,198Au production yields by 197Au neutron absorption for therapeutic purposes, Mater. Sci. Eng. C 68 (1) (2016) 449–454, https://doi.org/10.1016/j.msec.2016.06.018.
[28] A. Khorshidi, Accelerator-based methods in radio-material 99Mo/99 mTc production alternatives by Monte Carlo method: the scientific-expedient considerations in nuclear medicine, J. Multiscale Model. (JMM) 10 (1) (2018) 1930001, https://doi.org/10.1142/S1756973719300016.
[29] A. Khorshidi, Accelerator driven neutron source design via beryllium target and 208Pb moderator for boron neutron capture therapy in alternative treatment strategy by Monte Carlo method, J. Cancer Res. Ther. 13 (3) (2017) 456–465, https://doi.org/10.4103/0973-1482.179180.
[30] A. Khorshidi, M. Ashoor, Modulation transfer function assessment in parallel beam and fan beam collimators with square and cylindrical holes, Ann. Nucl. Med. 28 (4) (2014) 363–370, https://doi.org/10.1007/s12149-014-0820-2.
[31] ASTM E2862-18, Standard Practice for Probability of Detection Analysis for Hit/Miss Data, ASTM International, West Conshohocken, PA, 2018, https://doi.org/10.1520/E2862-18. www.astm.org.